Research Article

Adsorption Science & Technology
Volume 42: 1–21

DOI: 10.1177/02636174241285773
journals.sagepub.com/home/adt

Design of decolorization of methylene blue mixed synthetic wastewater via modified vermiculite using Taguchi method

Sahra Dandil
Department of Chemical Engineering, Faculty of Enginering, Bilecik Şeyh Edebali University, Bilecik, Türkiye

Abstract

In this study, vermiculite was modified and used in the decolorization of wastewater containing methylene blue. Taguchi experimental design method was applied to the process. An L_{16} orthogonal array was obtained according to Taguchi design by determining five factors effective on the process (pH, time, concentration, amount, and temperature) and four levels of these factors. Taguchi method determined concentration as the most effective factor. It suggested pH 3, 60 min, 5 $mg.L^{-1}$, 2 $g.L^{-1}$ and 50°C as optimum conditions. Equilibrium studies were carried out with Langmuir, Freundlich, Temkin, and Dubinin–Radushkevich isotherm models, and the process was found to be compatible with the Langmuir ($R^2 = 0.9103$) and Dubinin–Radushkevich ($R^2 = 0.9344$) model. It was determined that the material had a maximum capacity of 9.60 $mg.g^{-1}$. In kinetic studies conducted with pseudo-first-order, pseudo-second-order, and intraparticle diffusion models, the process complied with the pseudo-first-order ($R^2 = 0.9903$) and intraparticle diffusion ($R^2 = 0.9811$) models. The chemical composition was determined, and phase analysis was performed. By Branuer–Teller–Emmet analysis, it was determined that vermiculite exhibited a higher surface area (8.00 m^2/g) by modifying it. It was seen as a result of Fourier transform-infrared spectroscopy analysis that the active functional groups were similar for vermiculite and modified vermiculite. Mass losses of both materials were evaluated by thermal analysis.

Submitted August 17, 2024; accepted August 27, 2024

Corresponding author:
Sahra Dandil, Department of Chemical Engineering, Faculty of Enginering, Bilecik Şeyh Edebali University, 11100 Bilecik, Türkiye.
Email: sahra.ugur@bilecik.edu.tr

Keywords
clay, experimental design, modification, mineral, optimization

Introduction

Vermiculite is a natural clay mineral found abundantly in soil (Yang et al., 2024b; Shi et al., 2023). It stands out with its abundant reserves and low prices (Dai et al., 2023). It is a nontoxic, environmentally friendly substance with a specific gravity of approximately 2.2–2.4 and a pH of 7.0–7.5 (Ahmed et al., 2022; Bai et al., 2022; Çelik, 2023). It contains Si, Mg, Al, and Fe (Rehman et al., 2023). Its main structure is regular, consisting of an octahedral magnesium layer between two tetrahedral silica layers (Zhao et al., 2022). It contains exchangeable cations between its layers and contains water molecules and active hydroxyl groups (Qiaofang et al., 2024). Vermiculite has reactive surface regions, large surface area, and stable negative charge (Rind et al., 2024).

It is known that the negativity of clay minerals surfaces provides a high capacity to positive species and interfaces that can be replaced by cations in their structure (Patra et al., 2024). The unique structure of vermiculite provides it with a strong adsorption capacity (Wang et al., 2023). It has excellent cation exchange, expansion, and adsorption properties (Yuan et al., 2024). Based on these properties of vermiculite, researchers have studied neodymium adsorption/desorption using expanded vermiculite (de Vargas Brião et al., 2020), Pb(II) removal from aqueous solution by vermiculite subjected to chemical and thermal expansion (Hou et al., 2023), investigation of the ability of vermiculite modified with manganese oxide to remove Rhodamine B from aqueous solution (Chauke et al., 2024), investigating the adsorption potential of raw vermiculite and MnO_2 modified vermiculite in removing Ag^+ (Sarı and Tüzen, 2013), preparation of $Na^+/K^+/Mg^{2+}/Ca^{2+}$ expansion-modified vermiculite and calcination expansion-vermiculite to control metal emission (Yang et al., 2024a).

A dye is a coloring and ionizing organic substance (Singh et al., 2017). Colorants that originate from nature, such as plants, animals, or minerals, are called natural dyes (Pranta and Rahaman, 2024). Due to the low brightness and stability and fading in the presence of water and light of natural dyes, synthetic dyes, which are better in these areas, have come to the fore (Alegbe and Uthman, 2024). Dyes are generally grouped according to ionization (anionic, cationic, nonionic), dying method (basic, acidic, direct) and functional groups (azo, anthraquinone, indigoid, nitro, thiazine, xanthene, phthalein, etc.) (Sahu and Poler, 2024; Fattahi et al., 2024; Fang et al., 2024). The textile, plastic, cosmetic, and paper industries can be listed as the most common areas of use for dyes (Fideles et al., 2024). Especially after industrial use, the discharging of dye including wastewater into water resources causes serious environmental hazards (Meskel et al., 2024). Since they can be allergenic, carcinogenic, and mutagenic, they can negatively affect human life and threaten health (Balarak et al., 2020). Additionally, dyes including aromatic rings, such as methylene blue, are inert to heat, oxidizers, and light, and thus are difficult to remove from water (Oladipo et al., 2024). Methylene blue stands out especially in the dye industry for coloring silk, wool, cotton, and paper (Yusuf et al., 2024). Methylene blue, a cationic dye frequently used in many industries, has become an environmental problem due to its toxicity and nonbiodegradability (Vaddi et al., 2024; Din et al., 2024; Chouchane et al., 2024). This requires its effective removal (Valentini et al., 2023). Dye contaminants are eliminated from aqueous solutions by reverse osmosis, membrane, adsorption, etc. methods (Gadore et al., 2024).

In experimental studies with many variables and combinations, experimental design can be used to overcome the complexity and time-consuming (Durán et al., 2024). Experimental design methods provide design solutions as well as reduce costs and increase quality

(Googerdchian et al., 2018). Taguchi method is a statistical tool for designing experiments (Rahman and Raheem, 2022). It is an easy, efficient, and systematic method to optimize the design in terms of performance, quality, and cost (Yusuff et al., 2021). It provides the ability to predict optimum conditions and results (Lala et al., 2023). It also considers the interaction of factors (Patra et al., 2021). Taguchi method offers orthogonal arrays that allow the design to be executed with less experimentation (Dabagh et al., 2023). One of the main advantages is the use of orthogonal arrays that give equal importance to all levels and parameters (Lasu et al., 2024). They evaluate each factor to provide the output at optimum conditions with the minimum number of experiments for the specified factors, thereby reducing the time and cost required for the experiment (Egbosiuba et al., 2021; Korake and Jadhao, 2021).

The study involves the use of modified vermiculite mineral for effective decolorization of methylene blue mixed water. Vermiculite was prepared for the concentration value and modification conditions that Ren et al. (2022) had previously shown to have the highest adsorption capacity results for the removal of ammonia nitrogen from rare earth wastewater for the vermiculite they modified with NaCl solutions prepared at different concentrations. The novelty of this study is the decolorization of an aqueous solution containing methylene blue dye, which is a widely used and quite harmful component, using one of the frequently used and superior experimental design methods to save time, cost, and labor. Taguchi design was applied for the decolorization of methylene blue-containing water using modified vermiculite. By using Taguchi method, an orthogonal array was obtained for the determined process parameters, and effective factor determination, estimation of the results and optimization studies were carried out with the results of the experimental studies performed according to this array. The process was also considered by the ANOVA method, which statistically interprets the decolorization depending on the factors (Mustapha et al., 2021). The equilibrium state of the process was investigated with Langmuir, Freunlich, Temkin, and Dubinin–Radushkevich isotherms, and its kinetics was explained with pseudo-first-order, pseudo-second-order, and intraparticle diffusion models. pH at zero charge point was determined for modified vermiculite. The properties of vermiculite and modified vermiculite were revealed by XRF, XRD analysis, BET analysis, FTIR, and TGA.

Materials and methods

Experimental

Modification method. About 36 g NaCl (99.0–100.5%, Sigma-Aldrich) was added to 200 mL distilled water and mixed using a magnetic stirrer (IKA C-MAG HS 7). Then, 20 g of vermiculite (Agrenem) was added to the solution and allowed to mix at a constant speed for 24 h under ambient conditions. At the end of 24 h, it was washed four times with distilled water. After the last wash, it was dried in an oven (Mipro MLF 55) at 105°C overnight (Ren et al., 2022).

Method for pH at zero charge point. The determination of pH at the zero-charge point was carried out by rearranging a previous study (Faria et al., 2004). To determine the pH at zero charge point of modified vermiculite, 0.01 M NaCl solution was prepared. By taking 50 mL of this solution, the pH values were adjusted to between 1 and 12 with different concentrations of HCl (≥37%, Fluka) and NaOH (for analysis, Carlo Erba) solutions, and 0.05 g of modified vermiculite was added. After they were covered with parafilm and shaken (Memmert, WNB 22) at 210 rpm for 24 h under ambient conditions, the final pH values were measured.

Decolorization procedure. Taguchi experimental design method was applied for the experimental study of the decolorization of methylene blue-containing water using modified vermiculite. Stock methylene blue (for microscopy, Carlo

Erba) solution prepared at a concentration of 2000 mg.L^{-1} was used in the preparation of dye solutions. Experiments were carried out for 40 mL solution volumes. HCl and NaOH solutions were used to adjust pH. A shaking (Thermal H11960) speed of 210 rpm was used to perform decolorization studies. Before determining the absorbance values, centrifugation (Centurion Scientific, C2 series) was performed at 5000 rpm for 8 min. Determination of concentration values was achieved through ultraviolet-visible spectroscopy (Perkin Elmer, Elmer Analyst 800).

For the decolorization process, decolorization % and q were calculated using the following equations (Zolgharnein et al., 2013; Shokrollahzadeh et al., 2023; Lashgari et al., 2024):

$$\text{Decolorization } \% = \frac{(C_0 - C_t)}{C_0} \times 100 \quad (1)$$

$$q = \frac{(C_0 - C_e)V}{s} \quad (2)$$

Design of experiments. It was studied to determine the effect level of the factors, optimum conditions, and results for the decolorization of methylene blue mixed water using modified vermiculite by Taguchi method. Minitab 17 software was used for Taguchi method. For this process, five factors were determined: pH value of methylene blue solutions, contact time of methylene blue with modified vermiculite, methylene blue concentration, amount of modified vermiculite, and temperature of the experimental environment. Four levels were determined for each factor: pH (3, 4, 5, 6), time (15, 30, 45, 60 min), concentration (5, 10, 15, 20 mg.L^{-1}), amount (0.5, 1, 1.5, 2 g.L^{-1}), and temperature (20, 30, 40, 50°C). Each factor, notation, and level is listed in Table 1. The method provided an orthogonal array depending on the factors and their levels. For the determined factors and levels, 16 experimental studies were carried out according to the L_{16} (4^5) orthogonal array obtained in Taguchi design. Table 2 shows the orthogonal array of Taguchi system. The decolorization percentage values determined as a result of the experimental studies were defined as output to Taguchi system, and the evaluations of Taguchi system were obtained for the larger-the-better type of S/N ratio. The contributions of the factors selected for the decolorization process were determined. Contribution percentages were calculated with equation (3) (Shafizah et al., 2022):

$$\text{contribution } \% = \frac{SS_f}{SS_T} \times 100 \quad (3)$$

Modeling of the decolorization

Equilibrium modeling. The equilibrium state of the process of using modified vermiculite for the decolorization of methylene blue mixed water was examined with Langmuir, Freundlich, Temkin, and Dubinin–Radushkevich isotherm models. Equilibrium studies were carried out for 5–20 mg.L^{-1} methylene blue concentrations, at their pH value, for 60 min, 40 mL solution volume and 1 g.L^{-1} amount. The equations used for Langmuir, Freundlich, Temkin, and Dubinin–Radushkevich isotherm models are listed below (Nizam et al., 2024; Chen, 2015; Qais et al., 2023; Kutluay et al., 2019):

$$\text{Langmuir isotherm: } q_e = \frac{q_m K_L C_e}{1 + K_L C_e} \quad (4)$$

$$\text{Freundlich isotherm: } q_e = K_F C_e^{\frac{1}{n}} \quad (5)$$

$$\text{Temkin isotherm: } q_e = \frac{RT}{b_T} \ln(A_T C_e) \quad (6)$$

$$\text{Dubinin} - \text{Radushkevich isotherm: } q_e = q_m \exp(-\beta \varepsilon^2), \quad (7)$$

$$\varepsilon = RTln\left(1 + \frac{1}{C_e}\right) \quad (8)$$

$$E = \frac{1}{\sqrt{2\beta}} \quad (9)$$

Kinetic modeling. Kinetic examination of the decolorization process using modified vermiculite was carried out with pseudo-first-order, pseudo-second-order, and intraparticle diffusion models. For kinetic studies, the process was

Table 1. Selected factors and their levels.

Factor	Unit	Symbol	Level			
			Level 1	Level 2	Level 3	Level 4
pH		A	3	4	5	6
time	min	B	15	30	45	60
concentration	$mg.L^{-1}$	C	5	10	15	20
amount	$g.L^{-1}$	D	0.5	1	1.5	2
temperature	°C	E	20	30	40	50

monitored for 60 min for 10 $mg.L^{-1}$ methylene blue concentration, 1 g/L amount, and its pH value. Relevant equations are given below (Ibrahim et al., 2022; Choe et al., 2022; Huang et al., 2023):

$$\text{Pseudo-first-order:} q_t = q_e(1 - e^{-K_1 t}) \quad (10)$$

$$\text{Pseudo-second-order: } q_t = \frac{q_e^2 K_2 t}{1 + q_e K_2 t} \quad (11)$$

$$\text{Intra-particle diffusion:} q_t = K_{ip} t^{0.5} + C \quad (12)$$

Analytical procedure

XRF (Panalytical/Axios) analysis was applied to determine the elemental and oxide state composition of the materials. The crystalline structure was elucidated by XRD (Rigaku, SmartLab) analysis for 6 °/min and between 2 and 60° for 2Θ. BET (Micromeritics Surface Area and Porosity, Tristar II) analyzes were performed for unmodified and modified vermiculite samples. For BET analysis, degas was performed at 50°C for 12 h (Chauke et al., 2024; Long et al., 2014), and BJH pore width was determined by performing multipoint and pore analysis. The presence and types of active groups were determined by FTIR (Perkin Elmer, Spectrum 100) analysis. TGA (Exstar SII TGA/DTA 7200) was carried out similarly to a previous study in a nitrogen atmosphere, 10°C/min for between 30 and 1000°C (Feng et al., 2020).

Table 2. Orthogonal array for the decolorization process.

Experiment	Main factors				
	A	B	C	D	E
1	3	15	5	0.5	20
2	3	30	10	1	30
3	3	45	15	1.5	40
4	3	60	20	2	50
5	4	15	10	1.5	50
6	4	30	5	2	40
7	4	45	20	0.5	30
8	4	60	15	1	20
9	5	15	15	2	30
10	5	30	20	1.5	20
11	5	45	5	1	50
12	5	60	10	0.5	40
13	6	15	20	1	40
14	6	30	15	0.5	50
15	6	45	10	2	20
16	6	60	5	1.5	30

Results and discussion

Taguchi optimization

It was aimed to determine the optimum conditions and the effectiveness of the selected factors and their levels for the decolorization of methylene blue mixed wastewater using Taguchi design. Experiments are carried out according to the L_{16} orthogonal array of Taguchi method for five factors and four levels in Table 2. As a result, the decolorization percentage values and S/N ratios in Table 3 are obtained. Taguchi method

uses S/N to account for characteristic quality that deviates from the desired value (Duran-Jimenez et al., 2014). There are three types of S/N: nominal is best, smaller is better, and larger is better (Santra et al., 2014). These three types are being investigated depending on the statistically desired quality of responses (Mbachu et al., 2023). Since the highest decolorization was aimed with modified vermiculite, the larger the better option of S/N was chosen for this study (Varala et al., 2016). The S/N ratio plot showing the effectiveness of the determined factors for each level is given in Figure 1. Additionally, Figure 1 illustrates the optimum conditions for the decolorization. According to Figure 1, when modified vermiculite is used for the decolorization of methylene blue mixed water, the optimum conditions for the determined factors and their levels are A1 (pH3), B4 (60 min), C1 (5 $mg.L^{-1}$), D4 (2 $g.L^{-1}$), and E4 (50°C) according to the S/N ratios. Confirmation experiments were carried out for the optimum conditions determined by the design. For optimum conditions, 90.62% decolorization was obtained in the experimental study, and the predicted decolorization was found to be 97.61% in the design.

Table 4 represents the response table for S/N ratios. The rank values of decolorization, which show the effect of the factors, are also seen in the table. According to the rank values, it was determined that the initial methylene blue concentration (factor C) with rank level 1 was the most effective factor among the factors. Temperature (factor E) has rank 5 and is seen as the factor with the lowest effect.

ANOVA was performed to examine the relationship between the factors. A 95% confidence level was taken as the basis for analysis. ANOVA analysis results are given in Table 5. *F*-value and *p*-value data in Table 5 indicate the importance of the factors (Hussin et al., 2020). *F*-value expresses as the ratio of the mean square of the factor to the residual error (Tamang and Paul, 2022). Generally, if the *F*-value for a factor is above 3.13, the factor is determined to be effective (Abbasi et al., 2020). According to Olubunmi et al., the fit of the model and data or intense noise causes a high *F*-value, but in addition, if the *p*-value is below 0.05, it is explained that the *F*-value is not due to noise and a good fit is achieved (Olubunmi et al., 2020). A large *F*-value indicates a high contribution of the factor to the response (Baig et al., 2020). A factor is statistically significant when $p\text{-value} < 0.05$ (Rahman et al., 2023). Accordingly, factors A, C, and D seen in Table 5 are statistically significant. Factor C confirms its highest contribution with its maximum *F*-value and minimum *p*-value (Karaoglu and Yolcular, 2022).

Table 3. Decolorization % and S/N ratios for the orthogonal array.

Experiment	Decolorization %	S/N ratio (dB)
1	83.24	38.4065
2	95.39	39.5904
3	95.82	39.6289
4	98.26	39.8479
5	97.29	39.7613
6	99.23	39.9331
7	22.29	26.9611
8	64.21	36.1527
9	86.62	38.7527
10	45.61	33.1821
11	96.14	39.6584
12	61.17	35.7314
13	26.05	28.3154
14	27.40	28.7550
15	92.71	39.3424
16	83.08	38.3902

The contributions of factors A, B, C, D, and E on the decolorization process were determined. The percent contributions of the factors are given in Table 6. As seen in Table 6, C provides the largest contribution with 37.48%, while E has the lowest contribution for decolorization with 1.81%.

pH at zero charge point

pH is a measure of charge density. Attractive or repulsive interactions occur due to electrostatic interaction between charged molecules (Ahmad et al., 2023). Processes exhibit different adsorption behavior for varying pH values of the

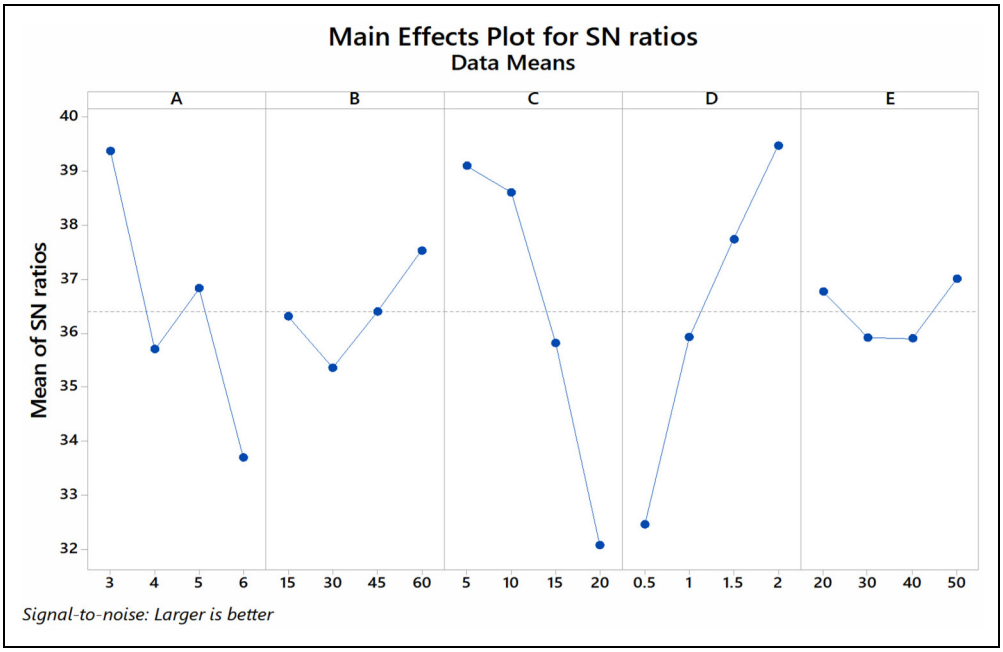

Figure 1. Main effects plot.

aqueous medium (Mamman et al., 2024). Since pH provides a charge to the medium, it affects the adhesion of the component in the aqueous medium to the solid material (Aragaw and Alene, 2022). Thus, it has been demonstrated by previous studies that changing capacity and percentage are obtained at varying pH values in adsorption processes (Yadav and Dasgupta, 2022). To present the relationship between pH and adsorption performance more clearly, pH at zero charge point needs to be examined (Agha et al., 2024). Zero charge point is a factor that expresses the pH sensitivity and the type of active centres of the material (Leng et al., 2015). A pH at zero charge point was determined for modified vermiculite. When the change in the difference between the final and initial pH values versus the initial pH values was examined, it was determined that the surface charge of the modified vermiculite was zero at a value of 1.03 (Mubarik et al., 2012). At this point, there is no electrostatic interaction (Liu et al., 2020). If the solution pH is higher than the pH at zero charge point, the material surface is negatively charged and can experience electrostatic attraction with positive charges (Li et al., 2020). Since the surface of the modified vermiculite was negatively charged at the pH values of 3, 4, 5 and 6 determined for the decolorization process, effective interaction with positive methylene blue was achieved.

Table 4. Response table for S/N ratios.

Level	A	B	C	D	E
1	39.37	36.31	39.10	32.46	36.77
2	35.70	35.37	38.61	35.93	35.92
3	36.83	36.40	35.82	37.74	35.90
4	33.70	37.53	32.08	39.47	37.01
Delta	5.67	2.17	7.02	7.01	1.10
Rank	3	4	1	2	5

Equilibrium modeling

The equilibrium dye concentration values and capacity values at varying initial methylene blue concentrations determined for the decolorization process are presented in Figure 2. Figure 3

Table 5. ANOVA results.

Factor	DOF	ADJ SS	ADJ MS	*F*-value	*p*-value
A	3	2632.4	877.47	11.99	0.035
B	3	256.3	85.42	1.17	0.451
C	3	4525.9	1508.65	20.61	0.017
D	3	4440.5	1480.17	20.22	0.017
Error	3	219.6	73.19		
Total	15	12074.7			

Table 6. Contribution of each factor.

Factor	Contribution %
A	21.80
B	2.12
C	37.48
D	36.77
E	1.81

contains graphs of Langmuir, Freundlich, Temkin, and Dubinin–Radushkevich isotherm models obtained from the equilibrium data of the decolorization process. Parameters of isotherm models that provide information about the equilibrium state are given in Table 7. It is seen that the R^2 values presented in Table 7 are higher for the Langmuir isotherm model than Freundlich model. This explains that the decolorization process of methylene blue mixed water using modified vermiculite is compatible with the Langmuir isotherm model. According to the Langmuir isotherm model, methylene blue molecules settle in a monolayer on the surface of modified vermiculite (Mamudu et al., 2023). Arrangement in a monolayer also implies that with the presence of a finite number of active sites, the layer will be saturated at a state and thus equilibrium will be reached (Alizadeh et al., 2024; Li et al., 2018; Syafiuddin et al., 2018). It also emphasizes that there is no lateral interaction between methylene blue molecules (Hung et al., 2023). The q_m value belonging to the Langmuir isotherm model determined as 9.60 $mg.g^{-1}$ represents the maximum capacity of modified vermiculite. As given in Table 7, Dubinin–Radushkevich isotherm model also seems to be compatible with the decolorization process. This model explains that the material surface has heterogeneous energy (Jan et al., 2021). The E value in Dubinin–Radushkevich isotherm model was calculated as 1.73 kJ/mol. The E value is less than 8 kJ/mol indicates the interaction of methylene blue with modified vermiculite through physical forces during the decolorization (Mostafapour et al., 2022).

Kinetic modeling

The progress of decolorization of methylene blue mixed wastewater over time was investigated and shown in Figure 4 in terms of changing methylene blue concentration. The graphs presented in Figure 5 belong to the kinetic models of the decolorization of methylene blue-containing water. Table 8 shows the parameters of the kinetic models. According to the table, the pseudo-first-order model was found to be more suitable for the process as it provided a higher R^2 value than the pseudo-second-order model. In addition, the experimental qe value of 8.53 $mg.g^{-1}$ was found to be closer to the first-order model than the pseudo-second-order model. The pseudo-first-order model provides information about the physical processing of decolorization (Ma et al., 2021). This physical interaction is reversible (Kadiri et al., 2021). It may also show that methylene blue molecules are located in a single layer on the modified vermiculite surface (Alalwan et al., 2021). It is seen from the table that the intraparticle model

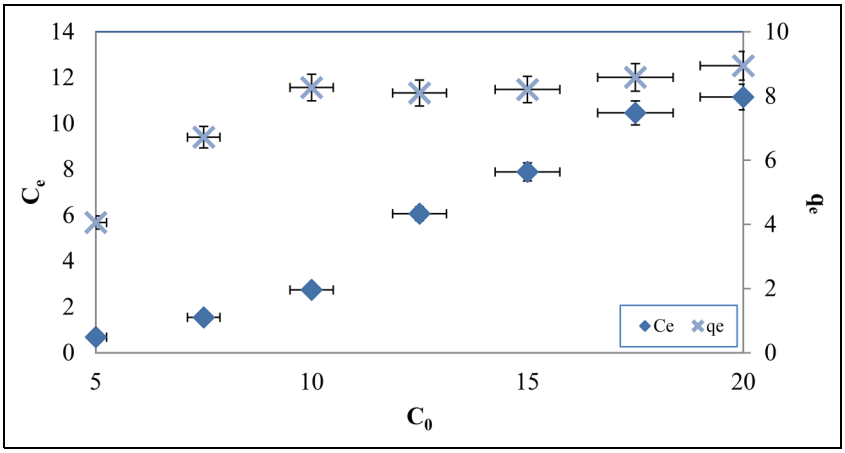

Figure 2. The equilibrium concentration and capacity values at varying initial concentrations.

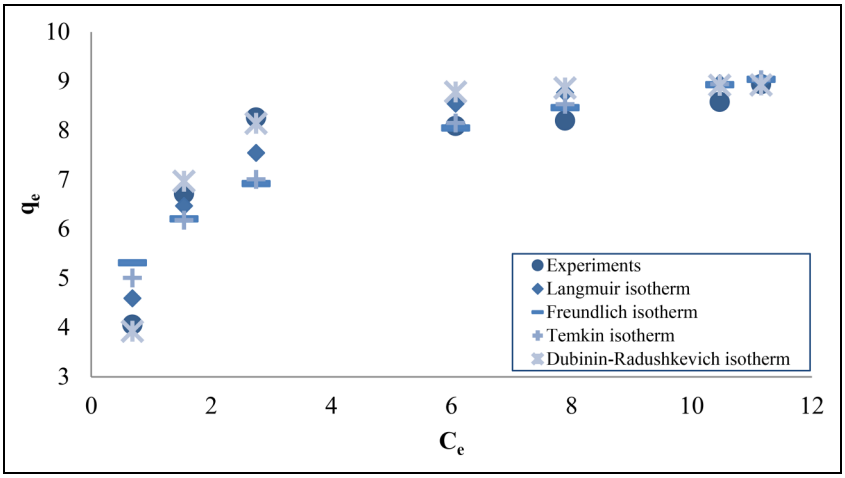

Figure 3. Isotherm plots.

Table 7. Isotherm model parameters.

Langmuir Isotherm Model			Freundlich Isotherm Model			Temkin Isotherm Model			Dubinin-Radushkevich Isotherm Model		
K_L	q_m	R^2	K_F	n	R^2	$b_T(x10^{-3})$	A_T	R^2	q_m	$\beta(x10^7)$	R^2
1.34	9.60	0.9103	5.71	5.25	0.7754	1.72	46.97	0.8239	8.99	1.67	0.9344

can explain decolorization. According to the intraparticle diffusion model curve (very close to the origin but does not pass through the origin), intraparticle diffusion is not the only effective step to control the rate (Azad et al., 2021; Zbair et al., 2019).

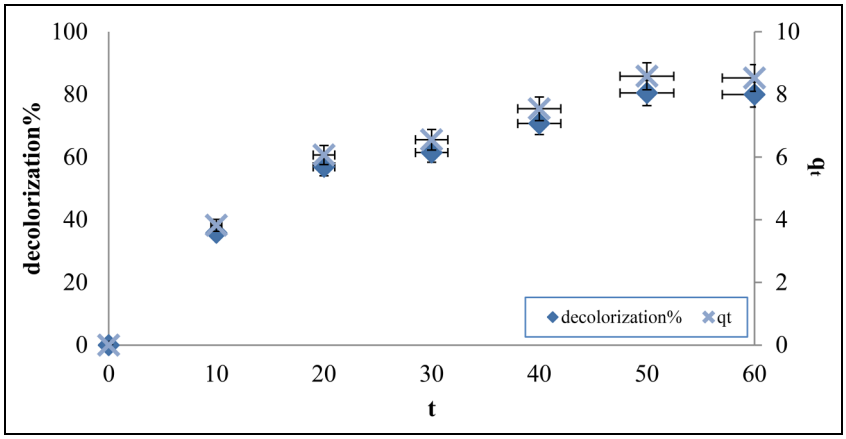

Figure 4. Progression of the decolarization over time.

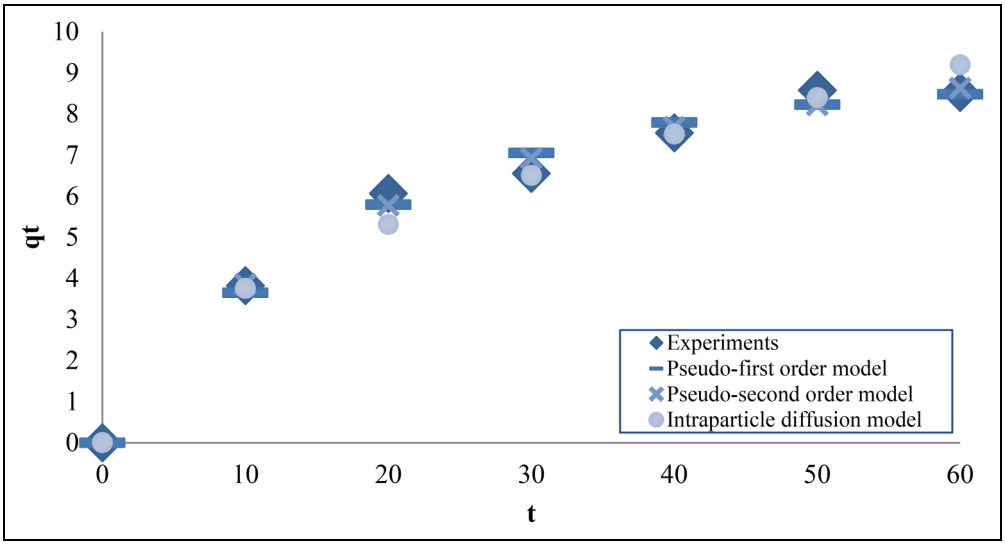

Figure 5. Kinetic model plots.

Table 8. Kinetic model parameters.

Pseudo-first-order Model			Pseudo-second-order Model			Intra-particle Diffusion Model		
$K_1(x10^2)$	q_e	R^2	$K_2(x10^3)$	q_e	R^2	K_{ip}	$C(x10^3)$	R^2
5.32	8.85	0.9903	4.43	11.46	0.9827	1.19	4.43	0.9811

Analytical assessment

Chemical composition. XRF analysis was performed to detect the elemental and oxide composition of vermiculite and its modified form. Table 9 shows the results for elemental and oxidized forms greater than 1%. According to Table 9, it was determined that Si, Mg, Al, and Fe, known as the main elements of vermiculite, were at the highest rates, respectively. It can be seen in the elemental results of modified vermiculite that percentage values for Na and Cl were obtained by modifying it using NaCl. It was determined that the decreasing composition percentage of the elements in oxide form for vermiculite was SiO_2, MgO, Al_2O_3, Fe_2O_3 and K_2O, respectively. For modified vermiculite, SiO_2, MgO, Al_2O_3 and Fe_2O_3, as well as Na_2O originating from the modification agent were found in the composition.

Table 9. XRF analysis results.

		Vermiculite	Modified Vermiculite
Element (%)	O	45.94	45.08
	Si	21.94	21.28
	Mg	17.48	16.73
	Al	7.014	6.99
	Fe	5.17	5.12
	Na	-	1.71
	Cl	-	1.11
Oxide (%)	SiO_2	46.95	45.53
	MgO	28.98	27.74
	Al_2O_3	13.25	13.20
	Fe_2O_3	7.39	7.32
	Na_2O	-	2.30
	Cl	-	1.11
	K_2O	1.06	-

Phase analysis. Crystalline phases for vermiculite and modified vermiculite were identified by XRD analysis (Figure 6). Vermiculite gave peaks at 6.102, 18.438, 24.662, 30.968 and 43.95° for 2Θ. These peaks indicate the characteristic vermiculite (002), hydrophlogopite, vermiculite, augite, and vermiculite, respectively (Luo et al., 2023; Yang et al., 2023; Hou et al., 2022b; Hou et al., 2022a). After modification, it gave peaks at 4.21, 7.211, 8.754, 29.231, 31.13 and 44.38° for 2Θ. The broad peak at 4.21° that appears with the modification indicates the presence of some irregular voids with an amorphous structure (Li et al., 2024). The 7.211° peak is the characteristic vermiculite peak (Rabello and da Conceição Ribeiro, 2021). The 8.754° peak indicates mica (Yang et al., 2023). Augite peak appeared at 29.231, 31.13 and 44. 38° (Hou et al., 2022b; Hou et al., 2022a).

Textural analysis. BET analysis was performed to investigate the surface area and pore width of vermiculite before and after modification. BET analysis results are listed in Table 10. As

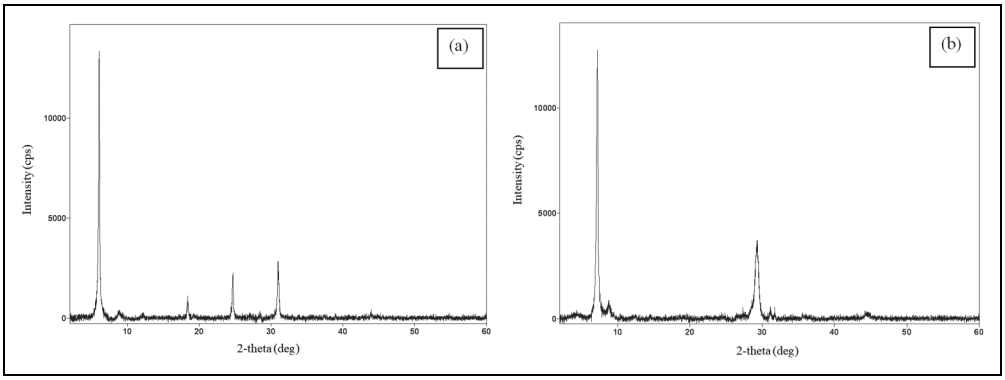

Figure 6. XRD patterns of (a) vermiculite and (b) modified vermiculite.

Table 10. BET analysis.

	BET Surface Area (m^2/g)	Langmuir Surface Area (m^2/g)	BJH Desorption Average Pore Width (nm)
Vermiculite	7.34	15.36	14.35
Modified vermiculite	8.00	20.00	11.30

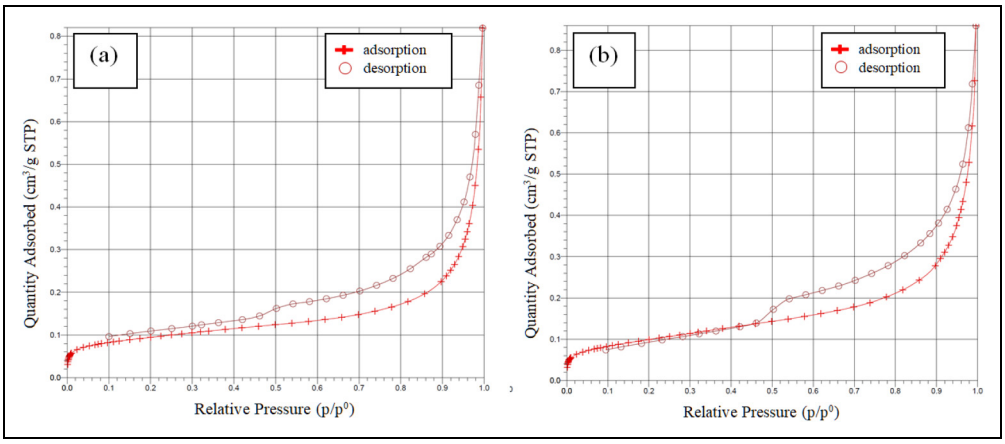

Figure 7. Nitrogen isotherms of (a) vermiculite and (b) modified vermiculite.

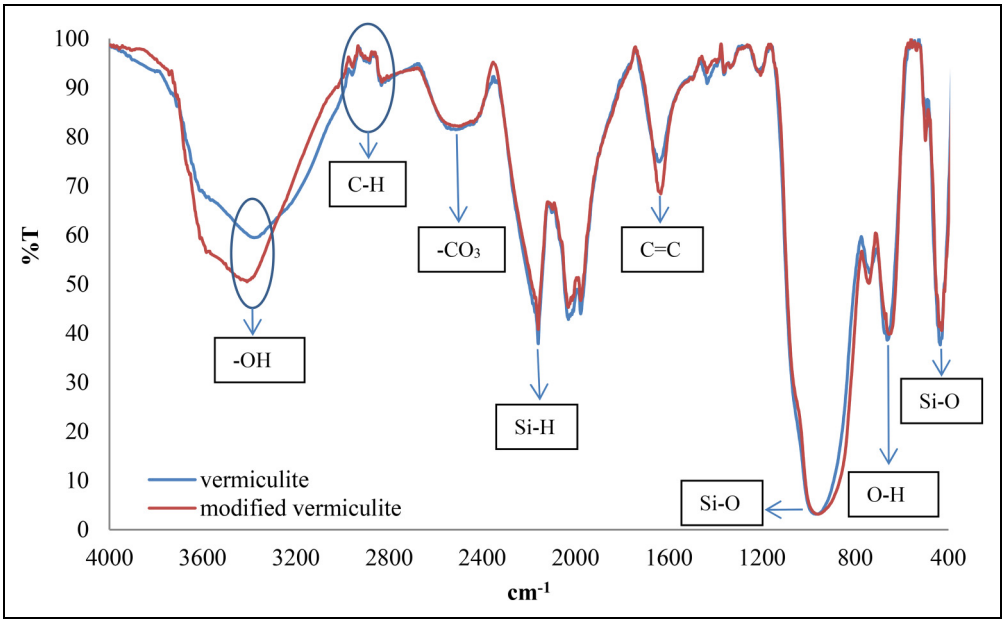

Figure 8. Infrared (IR) spectra.

Table 11. Functional group analysis.

Wave Number (cm^{-1})			
Vermiculite	Modified Vermiculite	Group	Reference
3378	3409	-OH	Okpara et al., 2020; Kohan Baghkheirati et al., 2016
2884	2956	C-H	Chang et al., 2010; Kaur et al., 2023; Soto-Vásquez et al., 2022
2833	2831		
2514	2500	$-CO_3$	Abdou et al., 2021; Miller and Wilkins, 1952; Legodi et al. 2001
2160	2160	Si-H	Thong-On et al., 2012
1640	1634	C=C	Sathya et al., 2018; Qin et al., 2020
968	959	Si-O	Linares, 2002
662	654	O-H	Liu and Kim, 2017; Sivaraman et al., 2015
435	429	Si-O	Avotina et al., 2023; Nenadović et al., 2023

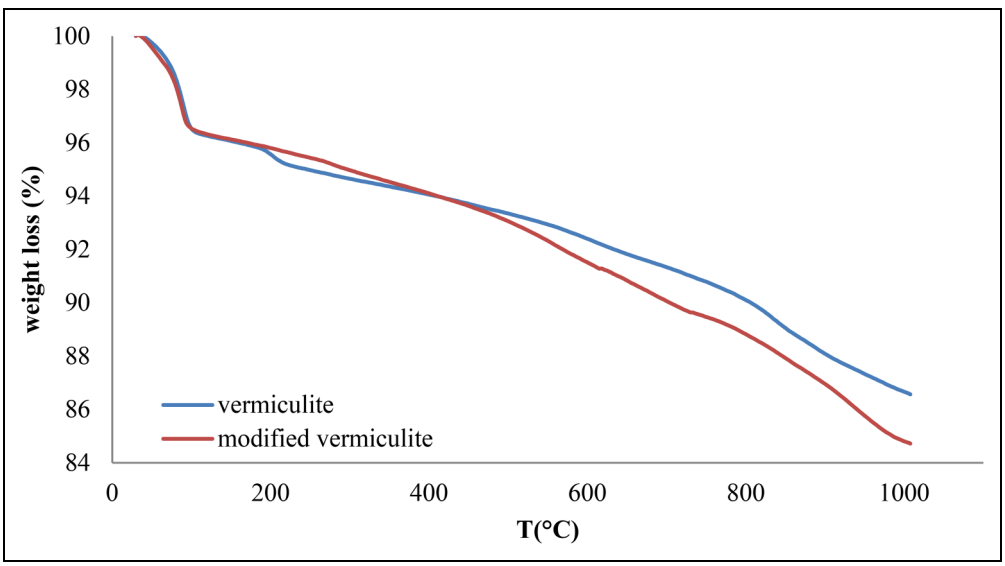

Figure 9. TGA curves.

seen in Table 10, vermiculite exhibited a higher BET surface area after the modification process was applied. Thus, modified vermiculite has become more suitable for decolorization than raw vermiculite. Additionally, pore width was found to be lower for modified vermiculite. Similar to Liu et al.'s study of biochar modified with $CaCl_2$, this may be due to the Na content in vermiculite modification (Liu et al., 2024).

Nitrogen adsorption/desorption isotherms of the vermiculite and modified vermiculite are given in Figure 7. Adsorption and desorption curves resulted in type IV isotherms and H3 hysteresis loop for both materials (Pang et al., 2021). Type IV isotherm and H3 hysteresis loop highlight the meso-sized and slit pores of vermiculite and its modified form (Brigante and Schulz, 2012; Behera et al., 2024).

Functional group analysis. FTIR spectra for vermiculite and modified vermiculite are seen in Figure 8. As seen in the figure, the FTIR spectra of vermiculite and modified vermiculite almost completely overlapped with very small changes in the locations and intensities of the peaks, and as a result, they were determined to have similar functional groups. In Table 11, the wave numbers at which peaks appear for vermiculite and modified vermiculite are given.

Thermal analysis. The weight change of vermiculite and modified vermiculite depending on temperature was followed by TGA, and the resulting graph is presented in Figure 9. Both materials exhibited weight loss due primarily to physically adsorbed water and initial hydration of interlayer cations (Marzec et al., 2021). The water remaining bound to the cations in the vermiculite interlayers was also removed by a second weight loss (Ma et al., 2019). Then, in the final stage of vermiculite and also seen in modified vermiculite, weight loss occurs due to dehydroxylation (Rama et al., 2019).

Conclusion

In this study, decolorization of wastewater containing methylene blue was carried out with vermiculite modified using NaCl. For decolorization, experiments were carried out related to Taguchi method and the L_{16} (4^5) orthogonal array obtained according to the design. Taguchi method listed the importance of factors as concentration > amount > pH > time > temperature. It presented that pH 3, 60 min, 5 mg.L^{-1}, 2 g.L^{-1} and 50°C conditions are optimum for the decolorization process. According to Langmuir isotherm, methylene blue molecules are settled in a single layer on the surface of the modified vermiculite, and Dubinin–Radushkevich isotherm indicates that this surface has heterogeneous energy regions. The pseudo-first-order kinetic model explained the reversible physical processing of decolorization. The intraparticle diffusion model is also involved in the decolorization. Si, Mg, Al, and Fe, the main elements of vermiculite and modified vermiculite, were detected by XRF analysis. Crystalline phases were identified by XRD analysis. BET analysis showed that by modifying vermiculite, the BET surface area increased and the pore size decreased. Nitrogen isotherms revealed meso-sized and slit pores of vermiculite and modified vermiculite. Quite similar functional groups of both materials were demonstrated by FTIR analysis. TGA was used for thermogravimetric examination of materials between 30 and 1000°C, and mass losses were identified.

Declaration of conflicting interests

The author declared no potential conflicts of interest with respect to the research, authorship, and/or publication of this article.

Funding

The author received no financial support for the research, authorship, and/or publication of this article.

ORCID iD

Sahra Dandil https://orcid.org/0000-0001-9724-5597

References

Abbasi F, Yaraki MT, Farrokhnia A, et al. (2020) Keratin nanoparticles obtained from human hair for removal of crystal violet from aqueous solution: Optimized by Taguchi method. *International Journal of Biological Macromolecules* 143: 492–500.

Abdou SM, Ali NA and Balboul MR (2021) Characterization of shale formation of abandoned petroleum wells and treatment using acid simulation technique. *Technology Audit and Production Reserves* 2(3(58)): 20–24.

Agha HM, Abdulhameed AS, Jawad AH, et al. (2024) Enhancing cationic dye removal via biocomposite formation between chitosan and food grade algae: Optimization of algae loading and adsorption parameters. *International Journal of Biological Macromolecules* 258: 128792.

Ahmad AA, Ahmad MA, Ali UFM, et al. (2023) Gasification char residues management:

Assessing the characteristics for adsorption application. *Arabian Journal of Chemistry* 16(9): 104993.

Ahmed A, Basfar S, Elkatatny S, et al. (2022) Vermiculite for enhancement of barite stability in water-based mud at elevated temperature. *Powder Technology* 401: 117277.

Alalwan HA, Mohammed MM, Sultan AJ, et al. (2021) Adsorption of methyl green stain from aqueous solutions using non-conventional adsorbent media: Isothermal kinetic and thermodynamic studies. *Bioresource Technology Reports* 14: 100680.

Alegbe EO and Uthman TO (2024) A review of history, properties, classification, applications and challenges of natural and synthetic dyes. *Heliyon* 10(13): e33646.

Alizadeh M, Akbari A, Abdoli SM, et al. (2024) Experimental investigation of sodium ion adsorption on polyacrylic acid grafted graphene oxide polymeric adsorbent: Kinetics, isotherms, and performance analyses. *Desalination* 580: 117551.

Aragaw TA and Alene AN (2022) A comparative study of acidic, basic, and reactive dyes adsorption from aqueous solution onto kaolin adsorbent: Effect of operating parameters, isotherms, kinetics, and thermodynamics. *Emerging Contaminants* 8: 59–74.

Avotina L, Goldmane AE, Zaslavskis A, et al. (2023) Estimation of thermal stability of Si-SiO2-W nanolayered structures with infrared spectrometry. *Materials* 17(1): 7.

Azad H, Mohsennia M, Cheng C, et al. (2021) Facile fabrication of PVB-PVA blend polymer nanocomposite for simultaneous removal of heavy metal ions from aqueous solutions: Kinetic, equilibrium, reusability and adsorption mechanism. *Journal of Environmental Chemical Engineering* 9(5): 106214.

Bai G, Luo F, Zou Y, et al. (2022) Effects of vermiculite on the growth process of submerged macrophyte Vallisneria spiralis and sediment microecological environment. *Journal of Environmental Sciences* 118: 130–139.

Baig U, Uddin MK and Gondal MA (2020) Removal of hazardous azo dye from water using synthetic nano adsorbent: Facile synthesis, characterization, adsorption, regeneration and design of experiments. *Colloids and Surfaces A: Physicochemical and Engineering Aspects* 584: 124031.

Balarak D, Al-Musawi TJ, Mohammed IA, et al. (2020) The eradication of reactive black 5 dye liquid wastes using Azolla filiculoides aquatic fern as a good and an economical biosorption agent. *SN Applied Sciences* 2: 1–11.

Behera AK, Shadangi KP and Sarangi PK (2024) Efficient removal of Rhodamine B dye using biochar as an adsorbent: Study the performance, kinetics, thermodynamics, adsorption isotherms and its reusability. *Chemosphere* 354: 141702.

Brigante M and Schulz PC (2012) Adsorption of the antibiotic minocycline on cerium (IV) oxide: Effect of pH, ionic strength and temperature. *Microporous and Mesoporous Materials* 156: 138–144.

Çelik Z (2023) Investigation of the use of ground raw vermiculite as a supplementary cement materials in self-compacting mortars: Comparison with class C fly ash. *Journal of Building Engineering* 65: 105745.

Chang H, Wang G, Yang A, et al. (2010) A transparent, flexible, low-temperature, and solution-processible graphene composite electrode. *Advanced Functional Materials* 20(17): 2893–2902.

Chauke L, Umejuru EC, RO A, et al. (2024) The removal of Rhodamine B from aqueous solution using manganese oxide modified vermiculite. *South African Journal of Chemical Engineering* 47(1): 159–168.

Chen X (2015) Modeling of experimental adsorption isotherm data. *Information* 6(1): 14–22.

Choe J, Ji J, Yu J, et al. (2022) Adsorption of Cr (VI) in aqueous solution by polypyrrole nanotube and polypyrrole nanoparticle; Kinetics, isotherm equilibrium, and thermodynamics. *Inorganic Chemistry Communications* 145: 109981.

Chouchane T, Abedghars MT, Chouchane S, et al. (2024) Improvement of the sorption capacity of methylene blue dye using slag, a steel by product. *Kuwait Journal of Science* 51(2): 100210.

Dabagh A, Benhiti R, Mohamed EH, et al. (2023) Application of Taguchi method, response

surface methodology, DFT calculation and molecular dynamics simulation into the removal of orange G and crystal violet by treated biomass. *Heliyon* 9(11): e21977.

Dai T, Feng J, Hwang JY, et al. (2023) High-efficiency removal of Cs (I) by vermiculite/zinc hexacyanoferrate (II) composite from aqueous solutions. *Journal of Environmental Chemical Engineering* 11(2): 109575.

de Vargas Brião G, da Silva MGC and Vieira MGA (2020) Neodymium recovery from aqueous solution through adsorption/desorption onto expanded vermiculite. *Applied Clay Science* 198: 105825.

Din MI, Khalid R, Hussain Z, et al. (2024) Synthesis and characterization of cobalt doped zinc oxide nanoparticles and their application for catalytic reduction of methylene blue dye. *Desalination and Water Treatment* 317: 100002.

Duran-Jimenez G, Hernandez-Montoya V, Montes-Moran MA, et al. (2014) Adsorption of dyes with different molecular properties on activated carbons prepared from lignocellulosic wastes by Taguchi method. *Microporous and Mesoporous Materials* 199: 99–107.

Durán JE, Bayarri B and Sans C (2024) Taguchi optimisation of the synthesis of vine-pruning-waste hydrochar as potential adsorbent for pesticides in water. *Bioresource Technology* 399: 130552.

Egbosiuba TC, Abdulkareem AS, Tijani JO, et al. (2021) Taguchi optimization design of diameter-controlled synthesis of multi walled carbon nanotubes for the adsorption of Pb (II) and Ni (II) from chemical industry wastewater. *Chemosphere* 266: 128937.

Fang W, Zhou Y, Cheng M, et al. (2024) A review on modified red mud-based materials in removing organic dyes from wastewater: Application, mechanisms and perspectives. *Journal of Molecular Liquids* 407: 125171.

Faria PCC, Orfao JJM and Pereira MFR (2004) Adsorption of anionic and cationic dyes on activated carbons with different surface chemistries. *Water Research* 38(8): 2043–2052.

Fattahi N, Fattahi T, Kashif M, et al. (2024) Lignin: A valuable and promising bio-based absorbent for dye removal applications. *International Journal of Biological Macromolecules* 276: 133763.

Feng J, Liu M, Fu L, et al. (2020) Enhancement and mechanism of vermiculite thermal expansion modified by sodium ions. *RSC Advances* 10(13): 7635–7642.

Fideles RA, Mageste AB, Nascimento LLBS, et al. (2024) Aqueous two-phase systems for the extraction, separation, and recovery of synthetic dyes. *TrAC Trends in Analytical Chemistry* 173: 117652.

Gadore V, Mishra SR, Yadav N, et al. (2024) Advances in zeolite-based materials for dye removal: Current trends and future prospects. *Inorganic Chemistry Communications* 166: 112606.

Googerdchian F, Moheb A, Emadi R, et al. (2018) Optimization of pb (II) ions adsorption on nano-hydroxyapatite adsorbents by applying Taguchi method. *Journal of Hazardous Materials* 349: 186–194.

Hou L, Xing B, Guo H, et al. (2023) Effect of mineralogical characteristics evolution of vermiculite upon thermal and chemical expansions on its adsorption behavior for aqueous Pb (II) removal. *Journal of Hazardous Materials* 430: 119040.

Hou L, Xing B, Kang W, et al. (2022a) Aluminothermic reduction synthesis of porous silicon nanosheets from vermiculite as high-performance anode materials for lithium-ion batteries. *Applied Clay Science* 218: 106418.

Hou L, Xing B, Zeng H, et al. (2022b) Aluminothermic reduction synthesis of Si/C composite nanosheets from waste vermiculite as high-performance anode materials for lithium-ion batteries. *Journal of Alloys and Compounds* 922: 166134.

Huang Y, Shen B, Zheng C, et al. (2023) Preparation of amphoteric double network hydrogels based on low methoxy pectin: Adsorption kinetics and removal of anionic and cationic dyes. *International Journal of Biological Macromolecules* 252: 126488.

Hung DQ, Dinh LX, Van Tung N, et al. (2023) The adsorption kinetic and isotherm studies of metal ions (Co^{2+}, Sr^{2+}, Cs^{+}) on Fe_3O_4 nanoparticle of radioactive importance. *Results in Chemistry* 6: 101095.

Hussin FNNM, Attan N and Wahab RA (2020) Taguchi design-assisted immobilization of Candida rugosa lipase onto a ternary alginate/

nanocellulose/montmorillonite composite: Physicochemical characterization, thermal stability and reusability studies. *Enzyme and Microbial Technology* 136: 109506.

Ibrahim SM, Ghanem AF, Sheir DH, et al. (2022) Effective single and contest carcinogenic dyes adsorption onto A-zeolite/bacterial cellulose composite membrane: Adsorption isotherms, kinetics, and thermodynamics. *Journal of Environmental Chemical Engineering* 10(6): 108588.

Jan SU, Ahmad A, Khan AA, et al. (2021) Removal of azo dye from aqueous solution by a low-cost activated carbon prepared from coal: Adsorption kinetics, isotherms study, and DFT simulation. *Environmental Science and Pollution Research* 28: 10234–10247.

Kadiri L, Ouass A, Hsissou R, et al. (2021) Adsorption properties of coriander seeds: Spectroscopic kinetic thermodynamic and computational approaches. *Journal of Molecular Liquids* 343: 116971.

Karaoglu S and Yolcular S (2022) Optimization of hydrogen generation process from the hydrolysis of activated Al–NaCl–SiC composites using Taguchi method. *International Journal of Hydrogen Energy* 47(66): 28289–28302.

Kaur P, Bohidar HB, Pfeffer FM, et al. (2023) A comparative assessment of biomass pretreatment methods for the sustainable industrial upscaling of rice straw into cellulose. *Cellulose* 30(7): 4247–4261.

Kohan Baghkheirati E, Bagherieh-Najjar MB, Khandan Fadafan H, et al. (2016) Synthesis and antibacterial activity of stable bio-conjugated nanoparticles mediated by walnut (Juglans regia) green husk extract. *Journal of Experimental Nanoscience* 11(7): 512–517.

Korake SR and Jadhao PD (2021) Investigation of Taguchi optimization, equilibrium isotherms, and kinetic modeling for cadmium adsorption onto deposited silt. *Heliyon* 7(1): e05755.

Kutluay S, Baytar O and Şahin Ö (2019) Equilibrium, kinetic and thermodynamic studies for dynamic adsorption of benzene in gas phase onto activated carbon produced from elaeagnus angustifolia seeds. *Journal of Environmental Chemical Engineering* 7(2): 102947.

Lala MA, Ntamu TE, Adesina OA, et al. (2023) Adsorption of hexavalent chromium from aqueous solution using cationic modified rice husk: Parametric optimization via Taguchi design approach. *Scientific African* 20: e01633.

Lashgari M, Khanahmadlou T and Naseri-Moghanlou S (2024) A coupled faradaic/electrostatic boosting strategy for decolorization of a refractory dye inside a dually-biased photoelectrochemical reactor: Time and energy saving. *Journal of Power Sources* 602: 234329.

Lasu CS, Muhamad M, Kamal NNSNM, et al. (2024) Assessing the performance of non-toxic nanomagnetic modified deep eutectic solvents for tetracycline adsorption: Taguchi approach for optimization. *Journal of Molecular Liquids* 399: 124374.

Legodi MA, De Waal D, Potgieter JH, et al. (2001) Rapid determination of CaCO3 in mixtures utilising FT-IR spectroscopy. *Minerals Engineering* 14(9): 1107–1111.

Leng L, Yuan X, Huang H, et al. (2015) Bio-char derived from sewage sludge by liquefaction: Characterization and application for dye adsorption. *Applied Surface Science* 346: 223–231.

Li K, Cai C, Zhou W, et al. (2024) Tandem pyrolysis-catalytic upgrading of plastic waste towards kerosene-range products using Si-pillared vermiculite with transition metal modification. *Journal of Hazardous Materials* 465: 133231.

Li X, Wang K and Peng Y (2018) Exploring the interaction of silver nanoparticles with pepsin and its adsorption isotherms and kinetics. *Chemico-Biological Interactions* 286: 52–59.

Li Y, Zhang X, Zhang P, et al. (2020) Facile fabrication of magnetic bio-derived chars by co-mixing with Fe3O4 nanoparticles for effective Pb2 +adsorption: Properties and mechanism. *Journal of Cleaner Production* 262: 121350.

Linares J (2002) Insights into the antigorite structure from Mössbauer and FTIR spectroscopies. *European Journal of Mineralogy* 14: 97–91.

Liu Y and Kim HJ (2017) Fourier transform infrared spectroscopy (FT-IR) and simple algorithm analysis for rapid and non-destructive assessment of developmental cotton fibers. *Sensors* 17(7): 1469.

Liu Y, Wang S, Huo J, et al. (2024) Adsorption recovery of phosphorus in contaminated water

by calcium modified biochar derived from spent coffee grounds. *Science of The Total Environment* 909: 168426.

Liu Y, Xu J, Cao Z, et al. (2020) Adsorption behavior and mechanism of Pb (II) and complex Cu (II) species by biowaste-derived char with amino functionalization. *Journal of Colloid and Interface Science* 559: 215–225.

Long H, Wu P, Yang L, et al. (2014) Efficient removal of cesium from aqueous solution with vermiculite of enhanced adsorption property through surface modification by ethylamine. *Journal of Colloid and Interface Science* 428: 295–301.

Luo W, Shi C, Wang S, et al. (2023) Carbon coated vermiculite aerogels by quick pyrolysis as cost-effective and scalable solar evaporators. *Desalination* 566: 116886.

Ma L, Su X, Xi Y, et al. (2019) The structural change of vermiculite during dehydration processes: A real-time in-situ XRD method. *Applied Clay Science* 183: 105332.

Ma X, Wang W, Sun C, et al. (2021) Adsorption performance and kinetic study of hierarchical porous Fe-based MOFs for toluene removal. *Science of The Total Environment* 793: 148622.

Mamman S, Abdullahi SSA, Birniwa AH, et al. (2024) Influence of adsorption parameters on phenolic compounds removal from aqueous solutions: A mini review. *Desalination and Water Treatment* 320: 100631.

Mamudu U, Alnarabiji MS and Lim RC (2023) Adsorption isotherm and molecular modeling of phytoconstituents from Dillenia suffruticosa leaves for corrosion inhibition of mild steel in 1.0M hydrochloric acid solution. *Results in Surfaces and Interfaces* 13: 100145.

Marzec A, Szadkowski B, Rogowski J, et al. (2021) Novel eco-friendly hybrid pigment with improved stability as a multifunctional additive for elastomer composites with reduced flammability and pH sensing properties. *Dyes and Pigments* 186: 108965.

Mbachu CA, Babayemi AK, Egbosiuba TC, et al. (2023) Green synthesis of iron oxide nanoparticles by Taguchi design of experiment method for effective adsorption of methylene blue and methyl orange from textile wastewater. *Results in Engineering* 19: 101198.

Meskel AG, Kwikima MM, Meshesha BT, et al. (2024) Malachite green and methylene blue dye removal using modified bagasse fly ash: Adsorption optimization studies. *Environmental Challenges* 14: 100829.

Miller FA and Wilkins CH (1952) Infrared spectra and characteristic frequencies of inorganic ions. *Environmental Challenges* 24(8): 1253–1294.

Mostafapour FK, Yilmaz M, Mahvi AH, et al. (2022) Adsorptive removal of tetracycline from aqueous solution by surfactant-modified zeolite: Equilibrium, kinetics and thermodynamics. *Desalination and Water Treatment* 247(8803540): 216–228.

Mubarik S, Saeed A, Mehmood Z, et al. (2012) Phenol adsorption by charred sawdust of sheesham (Indian rosewood; Dalbergia sissoo) from single, binary and ternary contaminated solutions. *Journal of the Taiwan Institute of Chemical Engineers* 43(6): 926–933.

Mustapha AN, Zhang Y, Zhang Z, et al. (2021) Taguchi and ANOVA analysis for the optimization of the microencapsulation of a volatile phase change material. *Journal of Materials Research and Technology* 11: 667–680.

Nenadović M, Ivanović M, Kisić D, et al. (2023) Changes in the physicochemical properties of geopolymer gels as a function of NaOH concentration. *Science of Sintering* 55(4): 509–519.

Nizam T, Krishnan KA, Joseph A, et al. (2024) Isotherm, kinetic and thermodynamic modelling of liquid phase adsorption of the heavy metal ions Zn (II), Pb (II) and Cr (VI) onto MgFe2O4 nanoparticles. *Groundwater for Sustainable Development* 25: 101120.

Okpara EC, Fayemi OE, Sherif ESM, et al. (2020) Green wastes mediated zinc oxide nanoparticles: Synthesis, characterization and electrochemical studies. *Materials* 13(19): 4241.

Oladipo AC, Aderibigbe AD, Olayemi VT, et al. (2024) Photocatalytic degradation of methylene blue using sunlight-powered coordination polymers constructed from a tetracarboxylate linker. *Journal of Photochemistry and Photobiology A: Chemistry* 448: 115331.

Olubunmi BE, Karmakar B, Aderemi OM, et al. (2020) Parametric optimization by Taguchi L9 approach towards biodiesel production from

restaurant waste oil using Fe-supported anthill catalyst. *Journal of Environmental Chemical Engineering* 8(5): 104288.

Pang P, Han H, Hu L, et al. (2021) The calculations of pore structure parameters from gas adsorption experiments of shales: Which models are better? *Journal of Natural Gas Science and Engineering* 94: 104060.

Patra BR, Nanda S, Dalai AK, et al. (2021) Taguchi-based process optimization for activation of agro-food waste biochar and performance test for dye adsorption. *Chemosphere* 285: 131531.

Patra K, Mittal VK, Bera S, et al. (2024) Role of Mg2 +and K+ ions in retention of radio-cesium (137Cs+) in vermiculite clay. *Journal of Hazardous Materials Advances* 13: 100411.

Pranta AD and Rahaman MT (2024) Extraction of eco-friendly natural dyes and biomordants for textile coloration: A critical review. *Nano-Structures & Nano-Objects* 39: 101243.

Qais DS, Islam MN, Othman MHD, et al. (2023) Nano-zinc oxide fibers: Synthesis, characterization, adsorption of acid blue 92 dye, isotherms, thermodynamics and kinetics. *Emerging Contaminants* 9(2): 100224.

Qiaofang F, Fangyu T and Ying W (2024) Preparation of vermiculite/g-C3N4/TiO2 composites and their degradation of dye wastewater. *Polyhedron* 247: 116713.

Qin Y, Qi F, Wang Z, et al. (2020) Comparison on reduction of VOCs emissions from radiata pine (Pinus Radiata D. Don) between sodium bicarbonate and ozone treatments. *Molecules* 25(3): 471.

Rabello LG and da Conceição Ribeiro RC (2021) A novel vermiculite/vegetable polyurethane resin-composite for thermal insulation eco-brick production. *Composites Part B: Engineering* 221: 109035.

Rahman N and Raheem A (2022) Graphene oxide/Mg-Zn-Al layered double hydroxide for efficient removal of doxycycline from water: Taguchi approach for optimization. *Journal of Molecular Liquids* 354: 118899.

Rahman N, Raheem A, Al-Kahtani AA, et al. (2023) Fractal-like kinetics for adsorption of Pb (II) on graphene oxide/hydrous zirconium oxide/crosslinked starch bio-composite: Application of Taguchi approach for optimization. *Journal of King Saud University-Science* 35(5): 102712.

Rama M, Eklund O, Fröjdö S, et al. (2019) Characterization of altered mica from Sokli, Northern Finland. *Clays and Clay Minerals* 67(5): 428–438.

Rehman WU, Rehman AU, Sharif QM, et al. (2023) Exfoliation characteristics of Swat vermiculite clay and its application in the preparation of light-weight composite panels. *Construction and Building Materials* 366: 130200.

Ren S, Huang S and Liu B (2022) Enhanced removal of ammonia nitrogen from rare earth wastewater by NaCl modified vermiculite: Performance and mechanism. *Chemosphere* 302: 134742.

Rind IK, Sarı A, Tuzen M, et al. (2024) Influential adsorption of Congo red using vermiculite/graphene/polyacrylamide composite. *Materials Chemistry and Physics* 314: 128804.

Sahu A and Poler JC (2024) Removal and degradation of dyes from textile industry wastewater: Benchmarking recent advancements, toxicity assessment and cost analysis of treatment processes. *Journal of Environmental Chemical Engineering* 12(5): 113754.

Santra D, Joarder R and Sarkar M (2014) Taguchi design and equilibrium modeling for fluoride adsorption on cerium loaded cellulose nanocomposite bead. *Carbohydrate Polymers* 111: 813–821.

Sarı A and Tüzen M (2013) Adsorption of silver from aqueous solution onto raw vermiculite and manganese oxide-modified vermiculite. *Microporous and Mesoporous Materials* 170: 155–163.

Sathya K, Saravanathamizhan R and Baskar G (2018) Ultrasonic assisted green synthesis of Fe and Fe/Zn bimetallic nanoparticles for invitro cytotoxicity study against HeLa cancer cell line. *Molecular Biology Reports* 45(5): 1397–1404.

Shafizah IN, Irmawati R, Omar H, et al. (2022) Removal of free fatty acid (FFA) in crude palm oil (CPO) using potassium oxide/dolomite as an adsorbent: Optimization by taguchi method. *Food Chemistry* 373: 131668.

Shi C, Luo W, Dong H, et al. (2023) Ultralow thermal conductivity of robust vermiculite aerogels fabricated by fast trivalent cation induced

nanosheet gelation. *Chemical Engineering Journal* 477: 147020.

Shokrollahzadeh S, Tayar S, Azizmohseni F, et al. (2023) Fungal decolorization of toxic Triphenylmethane dye by newly isolated Ganoderma fungi: Growth, enzyme activity, kinetics. *Bioresource Technology Reports* 24: 101654.

Singh K, Kumar P and Srivastava R (2017) An overview of textile dyes and their removal techniques: Indian perspective. *Pollution Research* 36(4): 790–797.

Sivaraman B, Radhika N, Das A, et al. (2015) Infrared spectra and chemical abundance of methyl propionate in icy astrochemical conditions. *Monthly Notices of the Royal Astronomical Society* 448(2): 1372–1377.

Soto-Vásquez MR, Alvarado-García PAA, Youssef FS, et al. (2022) FTIR characterization of sulfated polysaccharides obtained from Macrocystis integrifolia algae and verification of their antiangiogenic and immunomodulatory potency in vitro and in vivo. *Marine Drugs* 21(1): 36.

Syafiuddin A, Salmiati S, Jonbi J, et al. (2018) Application of the kinetic and isotherm models for better understanding of the behaviors of silver nanoparticles adsorption onto different adsorbents. *Journal of Environmental Management* 218: 59–70.

Tamang M and Paul KK (2022) Adsorptive treatment of phenol from aqueous solution using chitosan/calcined eggshell adsorbent: Optimization of preparation process using Taguchi statistical analysis. *Journal of the Indian Chemical Society* 99(1): 100251.

Thong-On B, Rutnakornpituk B, Wichai U, et al. (2012) Magnetite nanoparticle coated with amphiphilic bilayer surfactant of polysiloxane and poly (poly (ethylene glycol) methacrylate). *Journal of Nanoparticle Research* 14: 1–12.

Vaddi DR, Malla R and Geddapu S (2024) Magnetic activated carbon: A promising approach for the removal of methylene blue from wastewater. *Desalination and Water Treatment* 317: 100146.

Valentini F, Cerza E, Campana F, et al. (2023) Efficient synthesis and investigation of waste-derived adsorbent for water purification. Exploring the impact of surface functionalization on methylene blue dye removal. *Bioresource Technology* 390: 129847.

Varala S, Kumari A, Dharanija B, et al. (2016) Removal of thorium (IV) from aqueous solutions by deoiled karanja seed cake: Optimization using Taguchi method, equilibrium, kinetic and thermodynamic studies. *Journal of Environmental Chemical Engineering* 4(1): 405–417.

Wang R, Liu Y, Luo F, et al. (2023) Synergistic effect of vermiculite and submerged plants on lake sediments. *Water Biology and Security* 2(3): 100181.

Yadav BS and Dasgupta S (2022) Effect of time, pH, and temperature on kinetics for adsorption of methyl orange dye into the modified nitrate intercalated MgAl LDH adsorbent. *Inorganic Chemistry Communications* 137: 109203.

Yang H, Guo J, Chu L, et al. (2023) Self-assembly of Fe-MOF on vermiculite nanosheets with enhanced catalytic activity. *Applied Clay Science* 245: 107138.

Yang Y, Zhong Z, Du H, et al. (2024a) Experimental and theoretical study to control the heavy metals in solid waste and sludge during pyrolysis using modified expanded vermiculite. *Journal of Hazardous Materials* 463: 132885.

Yang Y, Zhong Z, Jin B, et al. (2024b) Effective stabilization of heavy metals in solid waste and sludge pyrolysis using intercalated-exfoliated modified vermiculite: Experiment and simulation study. *Waste Management* 178: 126–134.

Yuan S, Ge Y, Su P, et al. (2024) Green technology for carbon dioxide utilization: Vermiculite based hydrotalcite for methane dry reforming. *Journal of Environmental Chemical Engineering* 12: 112308.

Yusuf LA, Ertekin Z, Fletcher S, et al. (2024) Enhanced ultrasonic degradation of methylene blue using a catalyst-free dual-frequency treatment. *Ultrasonics Sonochemistry* 103: 106792.

Yusuff AS, Ajayi OA and Popoola LT (2021) Application of Taguchi design approach to parametric optimization of adsorption of crystal violet dye by activated carbon from poultry litter. *Scientific African* 13: e00850.

Zbair M, Anfar Z, Ahsaine HA, et al. (2019) Kinetics, equilibrium, statistical surface modeling

and cost analysis of paraquat removal from aqueous solution using carbonated jujube seed. *RSC Advances* 9(2): 1084–1094.

Zhao R, Hao S, Guo Z, et al. (2022) Porous vermiculite membrane with high permeance for carbon capture. *Journal of Membrane Science* 664: 121102.

Zolgharnein J, Asanjarani N and Shariatmanesh T (2013) Taguchi L16 orthogonal array optimization for Cd (II) removal using Carpinus betulus tree leaves: Adsorption characterization. *International Biodeterioration & Biodegradation* 85: 66–77.

Abbreviations

Full name	Abbreviation
a constant	β ($mol^2.J^{-2}$)
aluminum	Al
aluminium(III) oxide	Al_2O_3
analysis of variance	ANOVA
Barret–Joyner–Halenda	BJH
Branuer–Teller–Emmet	BET
calcium	Ca
calcium chloride	$CaCl_2$
chlorine	Cl
concentration at the beginning of the experiment	C_0 ($mg.L^{-1}$)
concentration at the equilibrium moment	C_e ($mg.L^{-1}$)
correlation coefficient	R^2
Fisher test	*F*-value
Fourier transform-infrared spectroscopy	FTIR
free energy	E ($J.mol^{-1}$)
Freundlich constant	K_F ($(mg.g^{-1})(L.mg^{-1})^{1/n}$)
greatest uptake capacity	q_m ($mg.g^{-1}$)
heterogeneity factor	n
hydrochloric acid	HCl
intercept	C (mg.g)
iron	Fe
iron(III) oxide	Fe_2O_3
Langmuir equilibrium constant	K_L ($L.mg^{-1}$)
lead	Pb
magnesium	Mg
magnesium oxide	MgO
manganese dioxide	MnO_2
mass	s (g)
Polanyi potential	ϵ ($J.mol^{-1}$)
potassium	K
potassium oxide	K_2O
probability	*p*-value
rate constant	K_1 (min^{-1})
rate constant	K_2 ($g.mg^{-1}.min^{-1}$)
rate constant	K_{ip} ($mg.g^{-1}.min^{-1}$)
signal-to-noise	S/N
silicon	Si
silicon dioxide	SiO_2
silver	Ag
sodium	Na
sodium chloride	NaCl
sodium hydroxide	NaOH
solution volume	V (L)
sum of the square of a factor	SS_f
sum of the square values of all factors	SS_T
Temkin constant	A_T ($L.mg^{-1}$)
Temkin constant	b_T ($J.mol^{-1}$)
thermogravimetric analysis	TGA
uptake capacity	q ($mg.g^{-1}$)
uptake capacity at equilibrium	q_e ($mg.g^{-1}$)
uptake capacity at time t	q_t ($mg.g^{-1}$)
X-ray fluorescence spectroscopy	XRF
X-ray diffraction	XRD